Hybridization and suppression of superconductivity in $CeFeAsO_{1-y}$: Pressure and temperature dependence of the electronic structure

Hitoshi Yamaoka,[1] Ignace Jarrige,[2] Atsushi Ikeda-Ohno,[2] Satoshi Tsutsui,[3] Jung-Fu Lin,[4] Nao Takeshita,[5,6] Kiichi Miyazawa,[5,6,7] Akira Iyo,[5,6,7] Hijiri Kito,[5,6] Hiroshi Eisaki,[5,6] Nozumu Hiraoka,[8] Hirofumi Ishii,[8] and Ku-Ding Tsuei[8]

[1]*Harima Institute, The Institute of Physical and Chemical Research (RIKEN), Sayo, Hyogo 679-5148, Japan*

[2]*Japan Atomic Energy Agency, SPring-8, 1-1-1 Kouto, Sayo, Hyogo 679-5148, Japan*

[3]*Japan Synchrotron Radiation Research Institute, Sayo, Hyogo 679-5198, Japan*

[4]*Department of Geological Sciences, Jackson School of Geosciences, The University of Texas at Austin, Austin, Texas 78712, USA*

[5]*Nanoelectronics Research Institute (NeRI), National Institute of Advanced Industrial Science and Technology (AIST), Tsukuba, Ibaraki 305-8562, Japan*

[6]*Transformative Research-Project on Iron Pnictides (TRIP), JST, 5, Sanbancho, Chiyoda, Tokyo 102-0075, Japan*

[7]*Department of Applied Electronics, Tokyo University of Science, 2641 Yamazaki, Noda, Chiba 278-3510, Japan*

[8]*National Synchrotron Radiation Research Center, Hsinchu 30076, Taiwan*

(Received 12 July 2010; revised manuscript received 23 August 2010; published 23 September 2010)

Pressure and temperature dependence of the electronic structure of superconducting (SC) $CeFeAsO_{1-y}$ and non-SC $CeFeAsO_{1-y}$ have been investigated using two complementary hard x-ray spectroscopic probes at the Ce L_3 edge, partial fluorescence yield x-ray absorption spectroscopy and resonant x-ray emission spectroscopy. With increasing pressure, the ratio between the intensity of the peak related to the f^0 (Ce^{4+}) state and that of the f^1 (Ce^{3+}) state, $I(f^0)/I(f^1)$, is found to increase continuously for both compounds, indicating a continuous increase in the Ce valence. The valence of non-SC $CeFeAsO_{1-y}$ is found to be slightly higher than that of SC $CeFeAsO_{1-y}$ in the entire pressure and temperature ranges of this study. The valence of $CeFeAsO_{1-y}$ around 6 GPa, where the superconductivity breaks down, is estimated to be ~3.0, but no change in the valence is observed upon cooling. The dependence of the interatomic distances on the concentration of oxygen vacancies is studied via extended absorption fine structure spectroscopy.

DOI: 10.1103/PhysRevB.82.125123 PACS number(s): 74.70.Tx, 74.25.Jb, 75.30.Mb

I. INTRODUCTION

High superconducting (SC) transition temperatures (T_C) of 16–56 K have recently been reported for the compound *Ln*FeAs(O,F) (*Ln*: lanthanide), which belongs to the so-called 1111 family.[1,2] Superconductivity occurs through electron doping to the FeAs layer, achieved through the substitution of F to the O site. Electron-doping induced superconductivity was also reported in O-deficient $LnFeAsO_{1-y}$, synthesized by using high-pressure techniques as it cannot be obtained at normal pressure.[3–5]

A study of the optimally doped $LaFeAsO_{0.89}F_{0.11}$ compound under pressure showed an enhancement of T_C up to 43 K at 4 GPa, while a further increase in pressure induces a decrease in T_C, ultimately resulting in the suppression of superconductivity at 30 GPa.[6–8] A similar behavior was observed in LaFePO, $SrFe_2As_2$, and $Fe_{1.01}Se$.[9–12] High-pressure studies for $CeFeAsO_{0.88}F_{0.12}$, $SmFeAsO_{0.85}$, $NdFeAsO_{1-y}$ at optimum doping level, and LiFeAs, however, showed a monotonic decrease in T_C under pressure.[13–17] A more anomalous behavior was found for some Ce-1111 systems in which the superconductivity is suddenly suppressed under pressure. This is the case for the oxygen-deficient systems $CeFeAsO_{1-y}$ (Ref. 18) around 4.5 GPa and $CeFeAsO_{0.7}F_{0.3}$ around 8.6 GPa.[19] Based on x-ray diffraction measurements, it has been suggested that the deviation from the tetragonal crystal structure[20,21] as well as the reduction in the lattice parameters[22] may be the cause of the decrease in T_C under pressure in the iron pnictides. Another key structural factor which is affected by the application of pressure is the pnictogen height from the FeAs plane.[23] The sudden suppression of the superconductivity in $CeFeAsO_{1-y}$ under pressure however is yet to be explained, as it is not induced by a change in the crystal structure.[16,18,24]

Non-SC CeFePO has the typical ZrCuSiAs-type crystal structure of a *Ln*-1111 system and shows heavy-fermion behavior. Interestingly, a relation between the hybridization of the Ce 4*f* states with the Fe 3*d* states and the quenching of the SC state was evidenced through a study of this compound using angle-resolved photoelectron spectroscopy.[25] A number of Ce compounds are characterized by an overlap between the 4*f* and the conduction 5*d* states near the Fermi level, most often resulting in mixed valence state. Application of high pressure can result in drastic modifications of this 4*f*-5*d* hybridization and in turn likely affect the Ce 4*f*-Fe 3*d* interaction. The fact that the sharp decrease in the SC transition in $CeFeAsO_{1-y}$ at high pressure cannot be explained solely based on structural considerations calls for a detailed study of the pressure-induced changes in the Ce electronic structure. With this as the focus of the experiments, we performed measurements of the pressure-induced changes in the Ce valence for two systems, SC $CeFeAsO_{1-y}$ and non-SC $CeFeAsO_{1-y}$. To carry this out, we used two complementary hard x-ray spectroscopic probes at the Ce L_3 edge, partial fluorescence yield x-ray absorption spectroscopy (PFY-XAS) and resonant x-ray emission spectroscopy (RXES).[26–32] The PFY-XAS technique yields spectra with sharper features than conventional absorption, offering a higher accuracy when deriving quantitative information such as the valence. We find that both the SC and the non-SC

samples show a gradual increase in the valence with pressure. The valence of the non-SC sample retains a slightly higher value than that of the SC one throughout the measured pressure range. Extended x-ray absorption fine structure (EXAFS) spectroscopy at room temperature was also performed for both compounds at the Fe *K* absorption edge.

II. EXPERIMENTS

Polycrystalline oxygen-deficient Ce-1111 samples, SC $CeFeAsO_{1-y}$ (T_C=40 K) and non-SC $CeFeAsO_{1-y}$, are synthesized by high-pressure and high-temperature method.[4,5,33] The SC compound is considered to be optimally doped. Based on a comparison of the lattice parameters with other similar systems,[34,35] we estimate the amount of oxygen vacancies to be $y \sim 0.1$ in the SC sample and $y \sim 0$ in the non-SC sample.

PFY-XAS and RXES measurements were performed at the Taiwan beamline BL12XU at SPring-8. The undulator beam was monochromatized by a pair of Si(111) crystals and focused to a size of 30(horizontal)$\times$30(vertical) μm^2 at the sample position using a toroidal and K-B mirrors. Incident photon energies are calibrated by using metal *K*-absorption edges of V and Cr. Incident photon flux was estimated to be about 7×10^{11} photons/s at 5.46 keV from the measurement by using a pin diode (type S3590–09). A Johann-type spectrometer equipped with a spherically bent Si(400) crystal (radius of about 1 m) was used to analyze the Ce $L\alpha_1$ ($3d_{5/2} \rightarrow 2p_{3/2}$) and Raman emissions with a solid-state detector (XFlash 1001 type 1201). The overall energy resolution was estimated to be about 1.5 eV around the emitted photon energy of 4.8 keV. The intensities of all spectra are normalized by the incident beam intensity monitored just before the target. A closed-circuit He cryostat was used for the low-temperature measurements. The high-pressure conditions were realized using a diamond-anvil cell with a Be gasket and the pressure-transmitting medium was silicone oil. The pressure was measured based on the Raman shift of the ruby fluorescence.

XAFS spectra were collected at Fe *K*-absorption edge at the beamline BL-27B of Photon Factory, High-Energy Accelerator Organization (KEK) in Tsukuba, using a Si(111) double-crystal monochromator. The measurement was performed in the fluorescence mode using a seven-element solid-state detector at room temperature and ambient pressure. The EXAFS data treatment, including the background (i.e., self-absorption effects) correction by Victoreen function, was performed according to a standard procedure[36] using the program WinXAS (version 3.2).[37] Theoretical EXAFS parameters (e.g., phase shifts or backscattering amplitudes) were calculated by the program FEFF 8.20 (Ref. 38) on the basis of the crystal structure of CeFeAsO.[21] Single scattering paths of Fe-As, Fe-Fe, and Fe-Ce were taken into account on the curve fitting to calculate their coordination numbers, interatomic distances, and Debye-Waller factors. The curve fitting was carried out both in the *k* space (EXAFS oscillation spectra) and *R* space (Fourier-transformed spectra). The amplitude reduction factors (S_0^2) were fixed at 0.9 for all the curve fittings in order to raise the precision of other parameters. The shifts in the threshold energy (ΔE_0) were left free to vary while constrained to be the same for all the scattering shells.

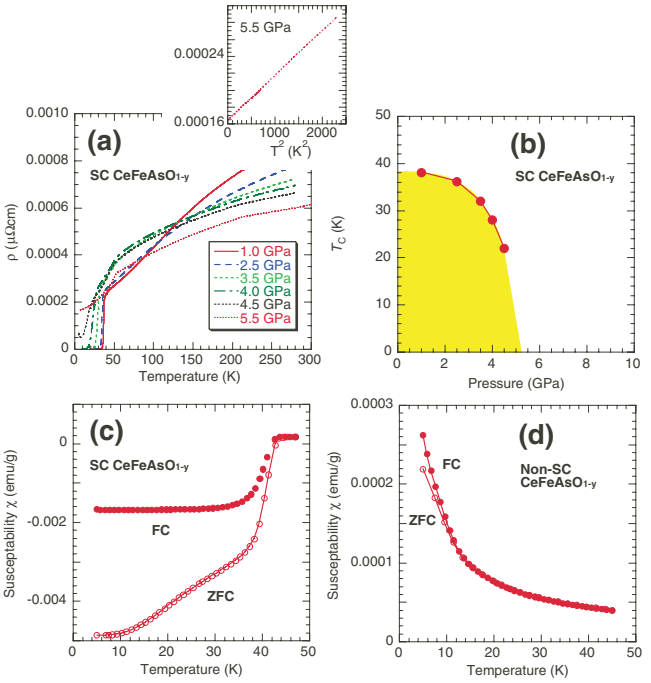

FIG. 1. (Color online) (a) Temperature (T) dependence of the resistivity at high pressures for SC $CeFeAsO_{1-y}$. Right-upper panel in (a) shows T^2 dependence of the resistivity. (b) Pressure dependence of the superconductor transition temperature (T_C; closed circles) for SC $CeFeAsO_{1-y}$. (c) Temperature dependence of the susceptibility for SC $CeFeAsO_{1-y}$. (d) Temperature dependence of the susceptibility for non-SC $CeFeAsO_{1-y}$. FC corresponds to measurements cooling the sample from 45 to 5 K under the magnetic field. ZFC is the cooling without field to 5 K and the measurement increasing the sample temperature from 5 to 45 K under the magnetic field.

III. RESULTS AND DISCUSSION

A. Resistivity, susceptibility, and x-ray diffraction

The pressure dependence of the resistivity and T_C is shown for SC $CeFeAsO_{1-y}$ in Figs. 1(a) and 1(b). T_C is seen to decrease rapidly under pressure below 4 GPa and the resistivity drop at low temperature is getting broader as the pressure is increased. At 4.5 GPa, the drop in the resistivity at low temperature remains, below which, however, the resistivity is no longer zero. Bulk superconductivity therefore disappears at this pressure. Nonetheless, for clarity, we plot the temperature corresponding to the onset of the resistivity drop at 4.5 GPa as T_C in Fig. 1(b). In contrast, in $CeFeAsO_{0.7}F_{0.3}$ a sudden drop of T_C was reported at 8.6 GPa, which was suggested to be a first-order transition coinciding with a 2% volume collapse.[19] In Nd-1111, no broadening of the resistivity drop was observed and T_C was found to decrease more slowly than Ce-1111 under pressure.[16,24] Since the carrier doping level is unchanged in underdoped Nd-1111 under pressure, it was concluded that the decrease in T_C is

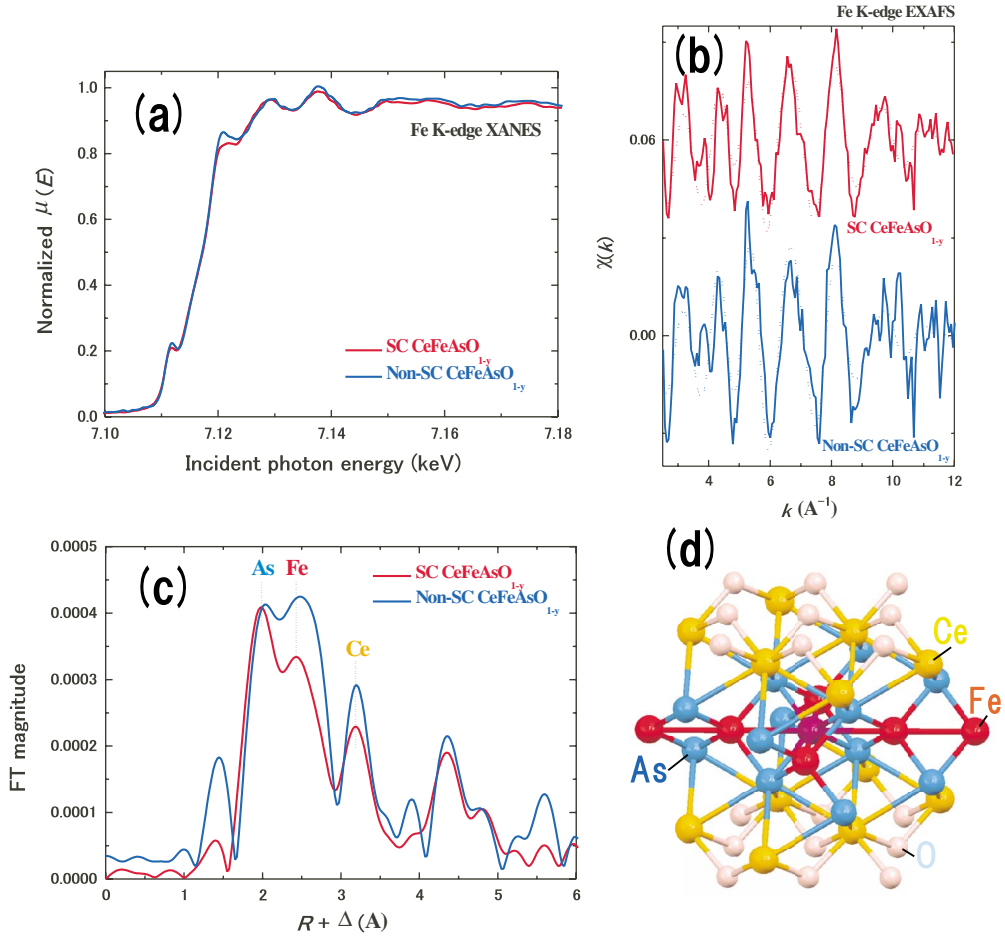

FIG. 2. (Color online) (a) XANES spectra at Fe K absorption edge for SC $CeFeAsO_{1-y}$ and non-SC $CeFeAsO_{1-y}$ at room temperature and ambient pressure. (b) EXAFS spectra as a function of k. Dashed lines are theoretical fits. (c) Fourier transforms of the Fe K edge EXAFS spectra in (b). Δ represents the phase shift, which is one of the theoretical parameters in the EXAFS formula. (d) Model of the crystal structure.

caused by the lattice contraction. Based on the differences with the results obtained for Ce-1111, Takeshita *et al.*[18] suggested that the suppression of the superconductivity in Ce-1111 is mainly of electronic origin. In our measurement the resistivity curves show a power law; the resistivity is proportional to $T^{1.196}$ ($50<T<130$ K) at 1.0 GPa, $T^{1.202}$ ($50<T<110$ K) at 2.5 GPa, $T^{1.357}$ ($32<T<50$ K) at 3.5 GPa, $T^{1.337}$ ($28<T<50$ K) at 4.0 GPa, $T^{1.429}$ ($28<T<50$ K) at 4.5 GPa, and $T^{2.000}$ ($7.5<T<48$ K) at 5.5 GPa. The right-upper inset in Fig. 1(a) shows the T^2 dependence of the resistivity at 5.5 GPa for SC $CeFeAsO_{1-y}$. In the pressure range where no superconductivity is observed, the system interestingly shows Fermi-liquid (FL) behavior. A similar behavior was observed for the chemical composition dependence of $BaFe_2(As_{1-x}P_x)_2$.[39] In the SC state, the resistivity showed a striking deviation from the FL behavior observed in the non-SC state. The FL behavior indicates the importance of the umklapp process when dealing with electron-electron scattering.[2]

Figures 1(c) and 1(d) show the magnetic susceptibility at low temperature. For SC $CeFeAsO_{1-y}$ diamagnetic behavior is clearly observed. The sharp drop of the susceptibility for both the zero-field cooling (ZFC) and the FC in SC $CeFeAsO_{1-y}$ corresponds to the onset of superconductivity while in non-SC $CeFeAsO_{1-y}$ no diamagnetic behavior is observed. From the Curie-Weiss fit for the FC susceptibility of non-SC $CeFeAsO_{1-y}$ at $20<T<45$ K the Weiss temperature and effective magnetic moments are estimated to be -8.07 K and 2.18 μ_B, respectively. The magnetic susceptibility is dominated by the localized Ce^{3+} moments.[40] But the value of the susceptibility is slightly smaller than the calculated 2.54 μ_B for Ce^{3+} according to the Hund theory. This result, along with the negative Weiss temperature, is indicative of the occurrence of f-d hybridization for Ce.

Using x-ray diffraction, the lattice parameters are estimated to be $a=3.990$ Å and $c=8.639$ Å for SC $CeFeAsO_{1-y}$, and $a=4.005$ Å and $c=8.642$ Å for non-SC $CeFeAsO_{1-y}$. In $NdFeAsO_{1-y}$ Eisaki *et al.*[33] showed that T_C depends on the oxygen content through the variation in the a-axis length. They estimated a boundary of $a=3.964$ Å between the SC and non-SC states with a smaller a-axis length favoring the SC state. For $LnFeAsO_{0.7}$ (Ln=Sm, Gd, Tb, and Dy) with fixed oxygen content, Miyazawa *et al.*[5] found the same trend for the relation between T_C and the a-axis length. Finally, in $LaFeAsO_{1-y}$ a similar result reported that superconductivity disappears at $a>4.03$ Å.[41] Our results on

TABLE I. EXAFS structural parameters obtained from the curve-fit analyses. The coordination numbers of As, Fe, and Ce are fixed to be 4, according to the crystal structure of CeFeAsO. The errors of the interatomic distance and Debye-Waller factor are ±0.01 Å and ±0.001 Å^2, respectively.

Sample	Shell	Distance (Å)	Debye-Waller factor (Å^2)
SC $CeFeAsO_{1-y}$	As	2.38	0.0058
	Fe	2.81	0.0139
	Ce	3.67	0.0110
Non-SC $CeFeAsO_{1-y}$	As	2.36	0.0069
	Fe	2.82	0.0096
	Ce	3.65	0.0074

$CeFeAsO_{1-y}$ are therefore consistent with all these previous reports on the *Ln*-1111 systems.

B. EXAFS

We investigated the structure of both compounds using EXAFS, which provides site-selective information about the local atomic structure around a selected absorbing atom through photoelectron scattering. Figure 2(a) shows the x-ray absorption near edge structure (XANES) spectra at the Fe *K* absorption edge for SC $CeFeAsO_{1-y}$ and non-SC $CeFeAsO_{1-y}$ at room temperature and ambient pressure. Figures 2(b) and 2(c) show the EXAFS spectra as a function of k (Å^{-1}) and their corresponding Fourier transforms (FTs), respectively. The structural parameters obtained from the fits are summarized in Table I. We assume that the coordination

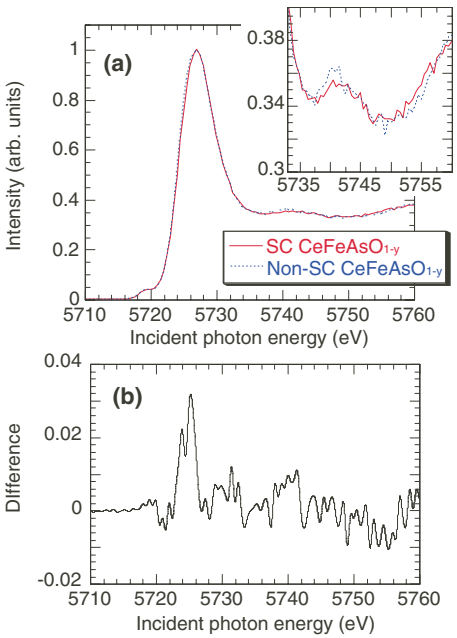

FIG. 3. (Color online) (a) PFY-XAS spectra at ambient pressure for SC $CeFeAsO_{1-y}$ and non-SC $CeFeAsO_{1-y}$. The measurements are performed at room temperature. (b) Difference of the intensities between two samples.

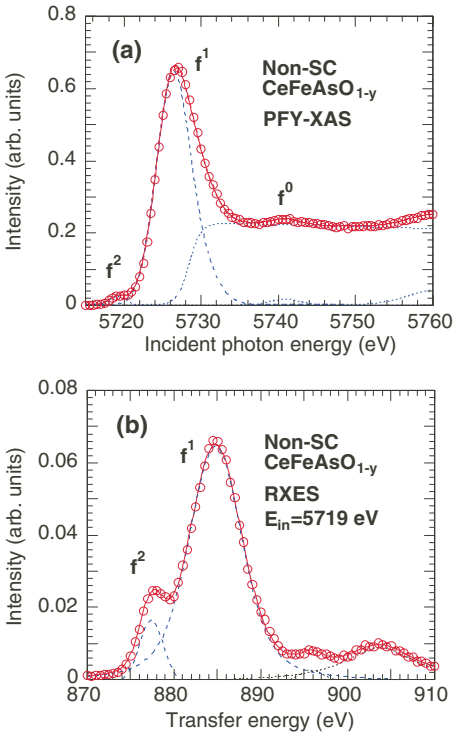

FIG. 4. (Color online) Examples of the curve fit for (a) PFY-XAS for non-SC $CeFeAsO_{1-y}$ and (b) RXES at E_{in}=5719 eV for SC $CeFeAsO_{1-y}$ at 300 K, respectively, where E_{in} is the incident photon energy. Open circles and solid line correspond to the experimental data and total intensity of fit curves, respectively.

arrangement around Fe is unchanged and thus the coordination number for Fe-As, Fe-Fe, and Fe-Ce remains equal to 4, according to the crystal structure of CeFeAsO.[21] The interatomic distances in Table I are the distances from the center Fe atom shown in Fig. 2(d). Three significant peaks are observed at around $R+\Delta=2.0$, 2.5, and 3.2 Å in the FT spectra, corresponding to the As, Fe, and Ce shells. The interatomic distances Fe-As and Fe-Ce are found to be smaller for non-SC $CeFeAsO_{1-y}$ than SC $CeFeAsO_{1-y}$. We note that the difference of the Fe-Fe distance between the SC and the non-SC samples is on par with the error of the measurement. The opening angle at the top of the Fe_4As tetrahedron is estimated to be 113.2° for SC $CeFeAsO_{1-y}$ and 115.33° for non-SC $CeFeAsO_{1-y}$ by using the relation of $\alpha=\pi-2\cos^{-1}(d_{\text{Fe-Fe}}/\sqrt{2}d_{\text{Fe-As}})$, where d is the distance between the atoms.[42] The Fe-As-Fe angle of the SC $CeFeAsO_{1-y}$ is closer to the perfect tetrahedron angle of 109.5° than that of the non-SC $CeFeAsO_{1-y}$, as suggested by Lee *et al.*[20] The vertical height of As from the Fe-Fe plane is about 1.31 Å for SC $CeFeAsO_{1-y}$ and 1.26 Å for non-SC $CeFeAsO_{1-y}$. Our results are consistent with the idea that T_C is maximum around the pnictogen height of 1.38 Å in the Fe-based SC.[23,43]

We note that there is considerable difference in the Debye-Waller factors, i.e., local fluctuation of bond lengths, on Fe-Fe and Fe-As bonds. The peak amplitude of the EXAFS-FT spectra is mainly related both to the coordination number and to the Debye-Waller factors. We have assumed that the local arrangement (=coordination number) around

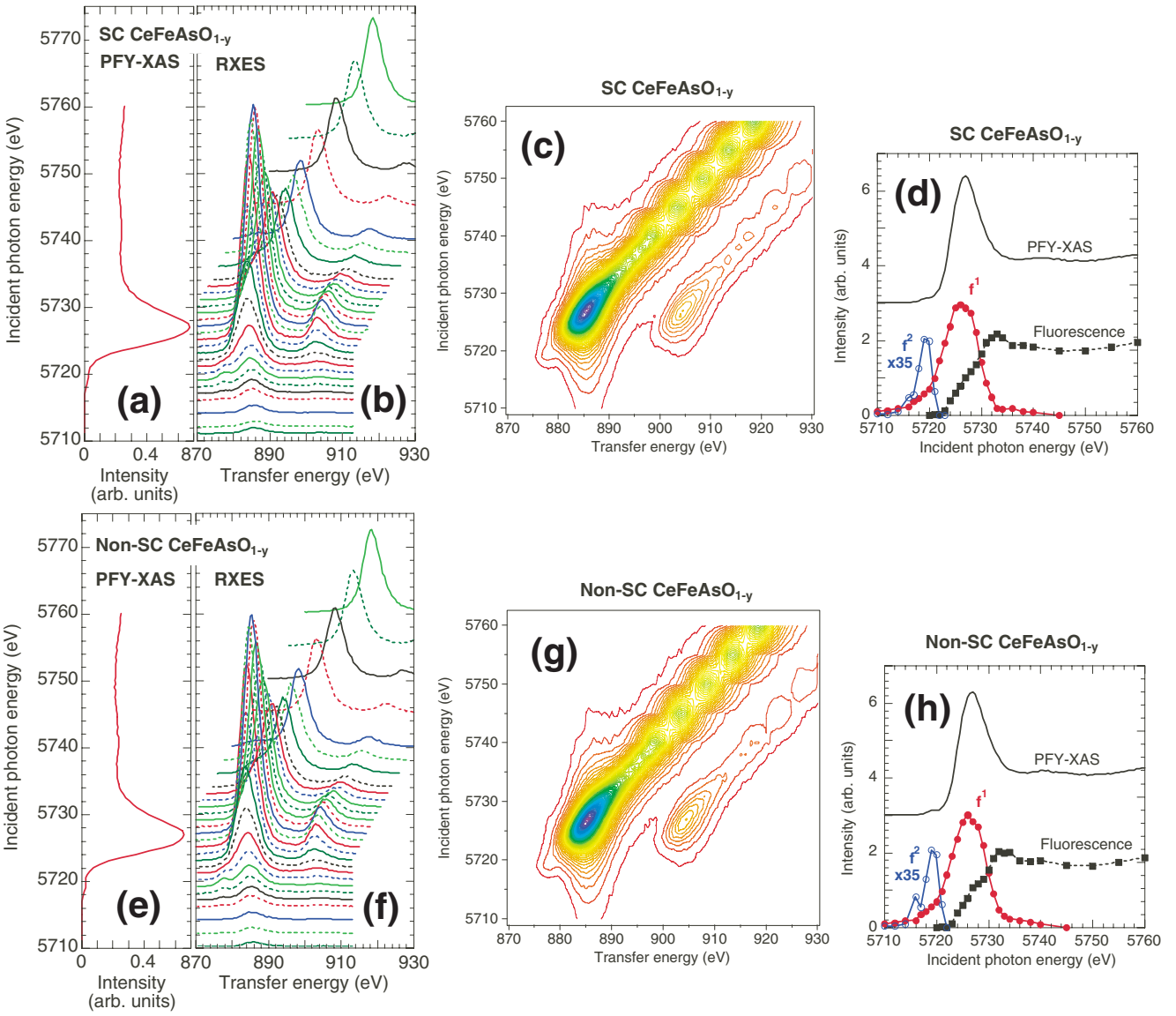

FIG. 5. (Color online) Upper panels: RXES spectra as a function of the incident photon energies with the PFY-XAS spectra for SC $CeFeAsO_{1-y}$ and non-SC $CeFeAsO_{1-y}$ at 300 K. The vertical offset of the RXES spectra in upper three panels corresponds to the incident energy in the PFY spectrum which they were collected at. Middle panels: contour images of the RXES spectra. Lower panels: analyzed results of the Raman and fluorescence components by the curve-fitting procedure. The intensity of f^2 component is multiplied by 35.

the Fe atom is unchanged regardless of the sample type, meaning that the observed differences in the EXAFS-FT amplitude on Fe-Fe and Fe-As shells originate mainly in the differences in Debye-Waller factors. Here we found that the Debye-Waller factor for the Fe-Fe bond is larger in the SC sample than in the non-SC sample at room temperature while that of As shows an opposite trend. The difference in Debye-Waller factor potentially originates either in the typical harmonic thermal vibration or the anharmonic vibration. Nonetheless, it was shown using nuclear resonant inelastic scattering on SC $LaFeAsO_{0.89}F_{0.11}$ and non-SC LaFeAsO that phonons are not the main mechanism that determines T_C.[44] The structural effects mentioned above, along with the electronic effects discussed in the next two sections, are seemingly more relevant to the superconductivity.

C. PFY-XAS and RXES: Ambient conditions

Figure 3(a) shows the PFY-XAS spectra obtained at ambient pressure for both SC and non-SC $CeFeAsO_{1-y}$ with an enlarged inset figure of $4f^0$ part. The intensity is normalized to the white line. In Fig. 3(b) the difference of the intensities for two samples is shown. The spectra show that both compounds are in the weakly mixed valence states, with the main component Ce^{3+} ($4f^1$) at E_{in}=5727 eV, and small fractions of Ce^{2+} ($4f^2$) at E_{in}=5719 eV and Ce^{4+} ($4f^0$) around E_{in} =5740 eV, where E_{in} is the incident photon energy. At ambient pressure the intensity of the $4f^0$ and $4f^1$ components in the spectrum of non-SC $CeFeAsO_{1-y}$ are observed to be, respectively, slightly higher and wider than those in SC $CeFeAsO_{1-y}$.

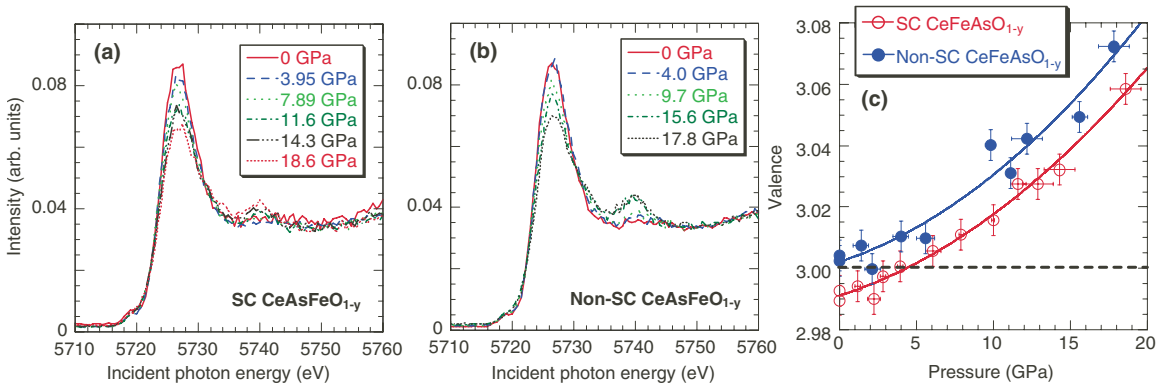

FIG. 6. (Color online) Pressure dependence of the PFY-XAS spectra and their analyzed results as a function of the pressure for SC $CeFeAsO_{1-y}$ and [(e) and (f)] non-SC $CeFeAsO_{1-y}$ at 300 K. Solid lines in (c) are fit curves assuming parabolic functions. Dashed line corresponds to the valence of 3.0.

To extract the intensity ratios of the different f components we have analyzed the PFY-XAS and RXES spectra.[26–31] Figure 4 shows examples of the fits for (a) the PFY-XAS spectrum and (b) the RXES spectrum at E_{in} =5719 eV measured for SC $CeFeAsO_{1-y}$ at 300 K. In the PFY-XAS spectra after subtraction of an arctangentlike (asymmetrical double sigmoid) function corresponding to the continuum excitations, two Voigt functions are used to fit the f^1 (Ce^{3+}) and the f^2 (Ce^{2+}) components. In the fit of the RXES spectra, we use a total of four Voigt functions for f^1 and f^2. We estimated the mean valence by using the formula $v=3+\{I(f^0)-I(f^2)\}/\{I(f^1)+I(f^2)+I(f^0)\}$.

The RXES spectra measured on SC $CeFeAsO_{1-y}$ and non-SC $CeFeAsO_{1-y}$ as a function of the incident energy across the Ce L_3 absorption edge are shown in Fig. 5 with the corresponding PFY-XAS spectra. The vertical offset of the RXES spectra in the panels (b) and (f) of Fig. 5 is scaled to the incident energy axis of the PFY spectra in the panels (a) and (e). The contour intensity maps of the RXES spectra are presented in the panels (c) and (g) of Fig. 5. Below the absorption edge we clearly observe the Raman like Ce^{2+} and Ce^{3+} peaks which remain at constant transfer energy. Above the edge, these progressively vanish at the expense of the fluorescence signal which shifts toward higher transfer energies when increasing the incident energy. Each spectrum is fitted with three components corresponding to the Raman 2 + and 3+ and the fluorescence as described above, and the results are shown in the panels (d) and (h) of Fig. 5. We note that the fit of the Ce^{4+} (f^0) component is rendered difficult because of its small intensity and the overlap with the strong fluorescence peak. We therefore chose to ignore this component in the fit.

D. PFY-XAS and RXES: Pressure and temperature dependences

The pressure dependence of the PFY-XAS spectra measured for SC $CeFeAsO_{1-y}$ and non-SC $CeFeAsO_{1-y}$ at 300 K is shown in Figs. 6(a) and 6(b), respectively. The PFY-XAS spectra are normalized by their own area after subtracting a constant background. We observe that, with increasing pressure, the intensity of f^1 decreases, while that of f^0 increases, and the ratio of f^0 to f^1 increases gradually. In the RXES spectra at E_{in}=5719 eV (not shown here) the changes in f^2 are small and the intensity ratio of f^2 to f^1 is found to increase slowly. Thus, the relative intensity of f^1 compared with those of f^0 and f^2 decreases with pressure.

We estimated the mean valence as a function of pressure using the same fitting procedure for the PFY-XAS spectra as described in Sec. III C. The corresponding results are shown in Fig. 6(c). The valence increases steadily with pressure for both samples and the valence of non-SC $CeFeAsO_{1-y}$ remains slightly higher than that of SC $CeFeAsO_{1-y}$ throughout the pressure range of this study.

It is noteworthy that the valence of SC $CeFeAsO_{1-y}$ around 4.5 GPa, where the superconductivity vanishes, reaches a value of 3.0, which is equal to the valence of the non-SC sample at ambient pressure. This suggests that the value of 3.0 may be regarded as the upper limit on the Ce valence for superconductivity to occur in $CeFeAsO_{1-y}$. Sun *et al.*[19] proposed the Ce $\gamma \rightarrow \alpha$ phase transition and the concomitant increase in the valence fluctuations as the origin of the disappearance of superconductivity. But our results show that the valence increases continuously for both non-SC and SC samples, and that the superconductivity disappears in SC $CeFeAsO_{1-y}$ without a phase transition. In the cuprate high-T_C superconductor of $YBa_2Cu_3O_7$, Pr substitution to the Y site suppresses the superconductivity.[29] The most commonly accepted idea is that the Pr-O hybridization destroys the superconductivity by binding the superconducting holes from the CuO_2 planes to tetravalent Pr sites. The situation could be similar for $CeFeAsO_{1-y}$, where the pressure-induced increase in the Ce valence indicates an increased supply of electrons to the FeAs superconducting layer, likely resulting in overdoping and ultimately the suppression of superconductivity.

The pressure dependence of the lattice parameters has been previously reported for $NdFeAsO_{1-y}$.[22] The parameters a and c decrease monotonically with pressure as well as the bond distances Fe-As, Nd-O, and Nd-As, while the changes in the As-Fe-As and Nd-O-Nd angles are very small, indicating that the crystal shape is maintained under pressure. A similar pressure dependence of the structure for $CeFeAsO_{1-y}$ is very likely with a monotonic lattice contraction causing the decrease in the pnictogen height and a negligible deviation from the tetragonal crystal structure.

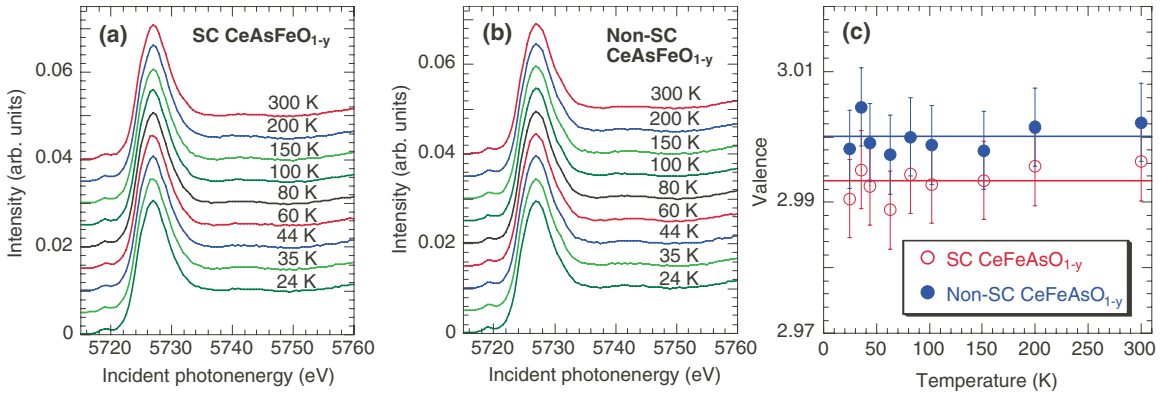

FIG. 7. (Color online) Temperature dependences of the PFY-XAS spectra and their analyzed results for SC $CeFeAsO_{1-y}$ and non-SC $CeFeAsO_{1-y}$ at ambient pressure. Solid lines in (c) are mean values of the valences.

Based on band calculations with the local-density approximation and dynamical mean-field theory, it was showed that in *Ln*FeAsO for *Ln*=Pr, Nd the 4*f* states did not interact with the Fe 3*d* band, whereas for *Ln*=Ce the 3*d*-4*f* hybridization was sufficiently strong for the Kondo screening of the 4*f* local moment to occur, possibly resulting in an enhancement of the valence fluctuations.[45,46] Under high pressure an exponential increase in the Kondo temperature (T_K) was predicted, T_K becoming comparable to T_C above 10 GPa. The band calculations qualitatively agree with our results that 3*d*-4*f* hybridization occurs in $CeFeAsO_{1-y}$ and increases with pressure. On the other hand, in the La-1111 system, which is considered not to show valence fluctuations, the enhancement of T_C was observed up to 4 GPa while a further increase in the pressure resulted in the gradual decrease in T_C.[6–8,17] Here we suggest that the superposition of the pressure-induced effects of the enhanced Ce hybridization and of the lattice contraction is responsible for the accelerated suppression of the superconductivity in the Ce-1111 system under high pressure compared with other *Ln*-1111 systems.

Figure 7 shows the temperature dependence of the PFY-XAS spectra for both samples with the estimated valences. No temperature dependence of the valence is observed for both samples, in agreement with the absence of temperature dependence of the crystal structure and bond distance previously reported in $LnFeAsO_{1-y}$.[20,47]

IV. CONCLUSION

We have performed an x-ray spectroscopic study on SC $CeFeAsO_{1-y}$ and non-SC $CeFeAsO_{1-y}$ by combining PFY-XAS, RXES, and EXAFS. The Ce valence of non-SC $CeFeAsO_{1-y}$ retains a slightly higher value than that of SC $CeFeAsO_{1-y}$ throughout the measured pressure and temperature ranges. The valence is found to increase monotonically with pressure for both samples. An upper limit of 3.0 is suggested for the valence, beyond which the superconductivity is suppressed. Our results imply that it is the combination under pressure of both the lattice contraction and the increased hybridization that may be responsible for the sudden suppression of the superconductivity at 4.5 GPa in $CeFeAsO_{1-y}$. Supporting this idea, is the progressive decrease in T_C previously reported in $NdFeAsO_{1-y}$, a system known to have a relatively weak 3*d*-4*f* hybridization. No temperature dependence of the valence is observed for both samples, in agreement with the nearly constant lattice parameters reported for $NdFeAsO_{1-y}$ upon cooling.

ACKNOWLEDGMENTS

The PFY-XAS and RXES experiments were performed at Taiwan beamline BL12XU (SPring-8 under Proposals No. 2009B4251 and No. 2009B4266, and NSRRC under Projects No. 2009-3-009-1 and No. 2009-3-009-2) at SPring-8. The Fe XAFS measurements at Photon Factory, KEK have been performed under the approval of the Photon Factory Advisory Committee (Proposal No. 2009G537). This work is partly supported by the RIKEN Harima Institute Director and RIKEN SPring-8 Center Director's Fund in 2008 and 2009, and by Grant in Aid for Scientific Researches under Grant No. 22540343 and on Innovative Areas under Grant No. 20102005 from Ministry of Education, Culture, Sports, Science and Technology of Japan. J.F.L. acknowledges support from the Energy Frontier Research under Extreme Environments (EFree), the U.S. National Science Foundation (Grant No. EAR-0838221) and the Carnegie/DOE Alliance Center (CDAC).

[1] Y. Kamihara, T. Watanabe, M. Hirano, and H. Hosono, J. Am. Chem. Soc. **130**, 3296 (2008).

[2] K. Ishida, Y. Nakai, and H. Hosono, J. Phys. Soc. Jpn. **78**, 062001 (2009), and references therein.

[3] Z. A. Ren, G. C. Che, X. L. Dong, J. Yang, W. Lu, W. Yi, X. L. Shen, Z. C. Li, L. L. Sun, F. Zhou, and Z. X. Zhao, EPL **83**, 17002 (2008).

[4] H. Kito, H. Eisaki, and A. Iyo, J. Phys. Soc. Jpn. **77**, 063707

(2008).
[5] K. Miyazawa, K. Kihou, P. M. Shirage, C.-H. Lee, H. Kito, H. Eisaki, and A. Iyo, J. Phys. Soc. Jpn. **78**, 034712 (2009).
[6] H. Takahashi, K. Igawa, K. Arii, Y. Kamihara, M. Hirano, and H. Hosono, Nature (London) **453**, 376 (2008).
[7] W. Yi, C. Zhang, L. L. Sun, Z. A. Ren, W. Lu, X. L. Dong, Z. C. Li, G. C. Che, J. Yang, X. L. Shen, X. Dai, Z. Fang, F. Zhou, and Z. X. Zhao, EPL **84**, 67009 (2008).
[8] C. W. Chu and B. Lorenz, Physica C **469**, 385 (2009).
[9] K. Igawa, H. Okada, K. Arii, H. Takahashi, Y. Kamihara, M. Hirano, H. Hosono, S. Nakano, and T. Kikegawa, J. Phys. Soc. Jpn. **78**, 023701 (2009).
[10] K. Igawa, H. Okada, H. Takahashi, S. Matsuishi, Y. Kamihara, M. Hirano, H. Hosono, K. Matsubayashi, and Y. Uwatoko, J. Phys. Soc. Jpn. **78**, 025001 (2009).
[11] H. Kotegawa, T. Kawazoe, H. Sugawara, K. Murata, and H. Tou, J. Phys. Soc. Jpn. **78**, 083702 (2009).
[12] S. Medvedev, T. M. McQueen, I. A. Troyan, T. Palasyuk, M. I. Eremets, R. J. Cava, S. Naghavi, F. Casper, V. Ksenofontov, G. Wortmann, and C. Felser, Nature Mater. **8**, 630 (2009).
[13] D. Zocco, J. Hamlin, R. Baumbach, M. Maple, M. McGuire, A. Sefat, B. Sales, R. Jin, D. Mandrus, J. Jeffries, S. Weir, and Y. Vohra, Physica C **468**, 2229 (2008).
[14] W. Yi, L. Sun, Z. Ren, W. Lu, X. Dong, H. Zhang, X. Dai, Z. Fang, Z. Li, G. Che, J. Yang, X. Shen, F. Zhou, and Z. Zhao, EPL **83**, 57002 (2008).
[15] C. W. Chu, R. P. Chaudhury, F. Chen, M. Gooch, A. Guloy, B. Lorentz, B. Lv, K. Sasmal, Z. Tang, L. Wang, and Y. Xue, J. Phys. Soc. Jpn. Suppl. C **77**, 72 (2008).
[16] N. Takeshita, A. Iyo, H. Eisaki, H. Kito, and T. Ito, J. Phys. Soc. Jpn. **77**, 075003 (2008).
[17] S. J. Zhang, X. C. Wang, R. Sammynaiken, J. S. Tse, L. X. Yang, Z. Li, Q. Q. Liu, S. Desgreniers, Y. Yao, H. Z. Liu, and C. Q. Jin, Phys. Rev. B **80**, 014506 (2009), and references therein.
[18] N. Takeshita, K. Miyazawa, A. Iyo, H. Kito, and H. Eisaki, J. Phys. Soc. Jpn. **78**, 065002 (2009).
[19] L. Sun, X. Dai, C. Zhang, W. Yi, L. Zheng, Z. Jiang, X. Wei, Y. Huang, J. Yang, Z. Ren, W. Lu, X. Dong, G. Che, Q. Wu, H. Ding, J. Liu, T. Hu, and Z. Zhao, arXiv:0907.4212 (unpublished).
[20] C. H. Lee, A. Iyo, H. Eisaki, H. Kito, M. T. Fernandez-Diaz, T. Ito, K. Kihou, H. Matsuhata, M. Braden, and K. Yamada, J. Phys. Soc. Jpn. **77**, 083704 (2008).
[21] J. Zhao, Q. Huang, C. de la Cruz, S. Li, J. W. Lynn, Y. Chen, M. A. Green, G. F. Chen, G. Li, Z. Li, J. L. Luo, N. L. Wang, and P. Dai, Nature Mater. **7**, 953 (2008).
[22] R. Kumai, N. Takeshita, T. Ito, H. Kito, A. Iyo, and H. Eisaki, J. Phys. Soc. Jpn. **78**, 013705 (2009).
[23] K. Kuroki, H. Usui, S. Onari, R. Arita, and H. Aoki, Phys. Rev. B **79**, 224511 (2009).
[24] N. Takeshita, T. Yamazaki, A. Iyo, H. Eisaki, H. Kito, T. Ito, K. Hirayama, H. Fukazawa, and Y. Kohori, J. Phys. Soc. Jpn. Suppl. C **77**, 131 (2008).
[25] M. G. Holder, A. Jesche, P. Lombardo, R. Hayn, D. V. Vyalikh, S. Danzenbächer, K. Kummer, C. Krellner, C. Geibel, Yu Kucherenko, T. K. Kim, R. Follath, S. L. Molodtsov, and C. Laubschat, Phys. Rev. Lett. **104**, 096402 (2010).
[26] I. Jarrige, H. Ishii, Y. Q. Cai, J.-P. Rueff, C. Bonnelle, T. Matsumura, and S. R. Shieh, Phys. Rev. B **72**, 075122 (2005).
[27] H. Yamaoka, M. Taguchi, A. M. Vlaicu, H. Oohashi, Y. Yokoi, D. Horiguchi, T. Tochio, Y. Ito, K. Kawatsura, K. Yamamoto, A. Chainani, S. Shin, M. Shiga, and H. Wada, J. Phys. Soc. Jpn. **75**, 034702 (2006).
[28] H. Yamaoka, N. Tsujii, K. Yamamoto, H. Oohashi, A. M. Vlaicu, K. Kunitani, K. Uotani, D. Horiguchi, T. Tochio, Y. Ito, and S. Shin, Phys. Rev. B **76**, 075130 (2007).
[29] H. Yamaoka, H. Oohashi, I. Jarrige, T. Terashima, Y. Zou, H. Mizota, S. Sakakura, T. Tochio, Y. Ito, E. Ya. Sherman, and A. Kotani, Phys. Rev. B **77**, 045135 (2008).
[30] H. Yamaoka, N. Tsujii, K. Yamamoto, A. M. Vlaicu, H. Oohashi, H. Yoshikawa, T. Tochio, Y. Ito, A. Chainani, and S. Shin, Phys. Rev. B **78**, 045127 (2008).
[31] H. Yamaoka, I. Jarrige, N. Tsujii, N. Hiraoka, H. Ishii, and K.-D. Tsuei, Phys. Rev. B **80**, 035120 (2009).
[32] H. Yamaoka, H. Sugiyama, Y. Kubozono, A. Kotani, R. Nouchi, A. M. Vlaicu, H. Oohashi, T. Tochio, Y. Ito, and H. Yoshikawa, Phys. Rev. B **80**, 205403 (2009).
[33] H. Eisaki, A. Iyo, H. Kito, K. Miyazawa, P. M. Shirage, H. Matsuhara, K. Kihou, C. H. Lee, N. Takeshita, R. Kumai, Y. Tomioka, and T. Ito, J. Phys. Soc. Jpn. Suppl. C **77**, 36 (2008).
[34] M. A. McGuire, R. P. Hermann, A. S. Sefat, B. C. Sales, R. Jin, D. Mandrus, F. Grandjean, and G. L. Long, New J. Phys. **11**, 025011 (2009).
[35] C. H. Lee *et al.* (unpublished).
[36] R. Prins and D. E. Koningsberger, *X-Ray Absorption: Principles, Applications, Techniques for EXAFS, SEXAFS, and XANES* (Wiley-Interscience, New York, 1988), p. 211.
[37] T. Ressler, J. Synchrotron Radiat. **5**, 118 (1998).
[38] A. L. Ankudinov, B. Ravel, J. J. Rehr, and S. D. Conradson, Phys. Rev. B **58**, 7565 (1998).
[39] S. Kasahara, T. Shibauchi, K. Hashimoto, K. Ikada, S. Tonegawa, R. Okazaki, H. Shishido, H. Ikeda, H. Takeya, K. Hirata, T. Terashima, and Y. Matsuda, Phys. Rev. B **81**, 184519 (2010).
[40] A. Jesche, C. Krellner, M. de Souza, M. Lang, and C. Geibel, New J. Phys. **11**, 103050 (2009).
[41] H. Mukuda, N. Terasaki, N. Tamura, H. Kinouchi, M. Yashima, Y. Kitaoka, K. Miyazawa, P. M. Shirage, S. Suzuki, S. Miyasaka, S. Tajima, H. Kito, H. Eisaki, and A. Iyo, J. Phys. Soc. Jpn. **78**, 084717 (2009).
[42] A. Iadecola, S. Agrestini, M. Filippi, L. Simonelli, M. Fratini, B. Joseph, D. Mahajan, and N. L. Saini, EPL **87**, 26005 (2009).
[43] Y. Mizuguchi, Y. Hara, K. Deguchi, S. Tsuda, T. Yamaguchi, K. Takeda, H. Kotegawa, H. Tou, and Y. Takano, Supercond. Sci. Technol. **23**, 054013 (2010).
[44] S. Higashitaniguchi, M. Seto, S. Kitao, Y. Kobayashi, M. Saito, R. Masuda, T. Mitsui, Y. Yoda, Y. Kamihara, M. Hirano, and H. Hosono, Phys. Rev. B **78**, 174507 (2008).
[45] L. Pourovskii, V. Vildosola, S. Biermann, and A. Georges, EPL **84**, 37006 (2008).
[46] H. M. Alyahyaei and R. A. Jishi, Phys. Rev. B **79**, 064516 (2009).
[47] C. J. Zhang, H. Oyanagi, Z. H. Sun, Y. Kamihara, and H. Hosono, Phys. Rev. B **78**, 214513 (2008).